

# A Feynman-Kac based numerical method for the exit time probability of a class of transport problems

Minglei Yang<sup>a</sup>, Guannan Zhang<sup>b</sup>, Diego del-Castillo-Negrete<sup>a</sup>, Miroslav Stoyanov<sup>b</sup>

<sup>a</sup>*Fusion Energy Division, Oak Ridge National Laboratory, Oak Ridge, TN.*

<sup>b</sup>*Computer Science and Mathematics Division, Oak Ridge National Laboratory, Oak Ridge, TN.*

---

## Abstract

The exit time probability, which gives the likelihood that an initial condition leaves a prescribed region of the phase space of a dynamical system at, or before, a given time, is arguably one of the most natural and important transport problems. Here we present an accurate and efficient numerical method for computing this probability for systems described by non-autonomous (time-dependent) stochastic differential equations (SDEs) or their equivalent Fokker-Planck partial differential equations. The method is based on the direct approximation of the Feynman-Kac formula that establishes a link between the adjoint Fokker-Planck equation and the forward SDE. The Feynman-Kac formula is approximated using the Gauss-Hermite quadrature rules and piecewise cubic Hermite interpolating polynomials, and a GPU accelerated matrix representation is used to compute the entire time evolution of the exit time probability using a single pass of the algorithm. The method is unconditionally stable, exhibits second order convergence in space, first order convergence in time, and it is straightforward to parallelize. Applications are presented to the advection diffusion of a passive tracer in a fluid flow exhibiting chaotic advection, and to the runaway acceleration of electrons in a plasma in the presence of an electric field, collisions, and radiation damping. Benchmarks against analytical solutions as well as comparisons with explicit and implicit finite difference standard methods for the adjoint Fokker-Planck equation are presented.

**Keywords:** Feynman-Kac formula, Fokker-Planck equation, stochastic differential equations, first exit time, adjoint equations, transport

---

## 1. Introduction

The study of transport is a top priority in science and engineering, as well as a source of applied mathematics and computational challenges. Some examples, among many others, include the quantification of the dispersal of pollutants in the atmosphere and the oceans, the design of efficient mixing protocols in chemical and mechanical engineering, and the study

---

**\*Notice:** This manuscript has been authored by UT-Battelle, LLC, under contract DE-AC05-00OR22725 with the US Department of Energy (DOE). The US government retains and the publisher, by accepting the article for publication, acknowledges that the US government retains a nonexclusive, paid-up, irrevocable, worldwide license to publish or reproduce the published form of this manuscript, or allow others to do so, for US government purposes. DOE will provide public access to these results of federally sponsored research in accordance with the DOE Public Access Plan.

of heat and particle transport in magnetically confined plasmas in controlled nuclear fusion [2, 5, 32]. The computation of the probability distribution of the first exit time, denoted by  $P(t, x)$ , is arguably one of the most natural and important transport problems [18, 3, 19]. That is the probability of a particle, with an initial condition  $x \in \mathbb{R}^d$ , to meet, for the first time, a specific target, e.g., reaching, or leaving, a region of the space before a predefined time  $t$ . The existence of probability distribution of the first exit time has been investigated in Refs. [38, 13]. One can find integral equations that can be used to compute this distribution numerically in Refs. [12, 26, 28, 33]. Asymptotic properties of the density are studied in Refs. [3, 14, 39]. Throughout this paper we restrict attention to Brownian motions, that is stochastic dynamical systems driven by a Wiener process which underlines the modeling of local transport in fluids and plasmas.

In Ref. [45], we presented a preliminary version of the method proposed here in the context of the “runaway acceleration” problem of electrons in magnetically confined fusion plasma for *time-independent* model parameters. In the present paper, we extend the method to time-dependent parameters, and most importantly to the computation of the full time evolution of the exit probability  $P(t, x)$ . Specifically, we present a method for the accurate approximation of  $P(t, x)$  for any  $t$  in an interval  $[0, T_{\max}]$  (rather than a fixed  $t$ ) in dynamic non-autonomous (i.e. with explicit time-dependent parameters) systems. The crux of the proposed new method, and the main difference with Ref. [45], is the computation of  $P(t, x)$  in  $[0, T_{\max}]$  with a single pass of the Feynman-Kac formula as described in Algorithm 1. An advantage of using the Feynman-Kac representation is that the resulting numerical scheme is *explicit* and *stable*. Implicit PDE solvers also have good stability properties but require solving the PDE  $N$  times in the non-autonomous case. When using explicit PDE solvers, one can combine  $N$  PDE solves into one. But, to guarantee stability the time step needs to be significantly reduced to guarantee stability. In summary, the proposed method significantly reduces the computational complexity of the full dynamics of the exit probability for non-autonomous problems, compared to both Ref. [45] and existing PDE solvers. Additional contributions of this work, beyond Ref. [45], include (i) illustrating the applicability of Feynman-Kac based scheme for 3D runaway electron problem in dynamic scenarios and fluid advection-diffusion problems in the presence of chaotic advection; and (ii) developing and demonstrating a GPU accelerated implementation, critical in solving large-scale problems.

These extensions, accompanied by significant mathematical and computational challenges per se, are motivated by critical physics and engineering application needs. For example, the modeling of runaway acceleration of electrons in realistic plasma physics systems requires the incorporation of high-dimensional (up to 6-dimensions) transport effect resulting from adding spatial transport and full-orbit dynamics in configuration space to the previously studied (see e.g., Ref. [40, 11, 9]) 2-dimensional transport in velocity space. Applications also underscore the need to extend the models to full time dependence. For example, plasmas and fluids are typically far-from-equilibrium and realistic modeling in dynamic scenarios requires the incorporation of time dependent parameters in the SDEs describing these systems. The evolution of these parameters can be given a priori or determined through a self-consistently coupling of the SDEs with another mathematical model, e.g., a system of partial differential equations (PDEs) describing the dynamics of the parameters. The results of this paper offer a first step to meet these challenges, and as illustration we apply the method to a time-dependent runaway electron problem in 3D (i.e., including spatial transport) and to a fluid

mixing problem involving chaotic advection on a time dependent cellular incompressible flow.

A standard numerical method for computing the exit probability is Monte Carlo (MC) (e.g., [7, 18, 4]), which simulates the subsequent positions of a path by time-stepping schemes and perform the statistics of the exit condition on a large ensemble of  $N$ -sample paths for each initial condition of interest [8, 20]. The main drawback of the MC method is the unfavorable scaling,  $\mathcal{O}(1/\sqrt{N})$ , of the statistical sampling error with the number of samples,  $N$ . Among the PDE based numerical approaches, the exit probability can be computed by first solving the forward Fokker-Planck equation [31, 42, 36, 25] associated with the SDE, and then convolve the probability density function of SDE solution with the exit condition.

Both the MC method and the PDE method for the forward Fokker-Planck equation depends on the initial condition. When studying the dependence of the probability of the exit time on large families of initial conditions, which is a problem of interest in scientific applications, these methods are not efficient since they require running the algorithm repeatedly. As it will be explained below, our method overcomes this limitation because the Feynman-Kac formula provides a type of Green's function representation for the exit time probability, from which the exit probability can be obtained by convolution with the initial condition.

An alternative approach is to solve the backward (adjoint) Fokker-Planck equation associated with the SDE [15, 6, 43, 27]. This method reduces the computation of the probability of exit time to the solution of a terminal-value problem of a parabolic PDE. Although superior to MC sampling, the adjoint methods share the limitations of PDE solvers including numerical instability, poor scalability with dimensions, and algorithmic challenges in parallelization. Also, since the adjoint methods are based on the solution of a terminal-value problem, in principle they only provide  $P(t, x)$  for a fixed  $t$ . That is, computing  $P(t, x)$  for  $t \in \{t_1, t_2, \dots, t_M\}$  requires to solve the adjoint problem  $M$ -times.

We propose a different method based on the direct approximation of the Feynman-Kac formula that establishes the connection between the solution of the (backward) adjoint Fokker-Planck equation and the associated forward SDEs. We express the stochastic representation of the solution of the adjoint equation as mathematical expectations and compute these expectations using Gauss-Hermite quadrature rules and piecewise cubic Hermite interpolating polynomials (PCHIP). Three quadrature points in each dimension are sufficient to guarantee first order,  $\Delta t$ , global convergence in time. The shape-preserving PCHIP interpolation guarantees that all the interpolated values are between 0 and 1. To avoid direct approximation of the random exit time, we exploit the regularity of the exit probability [41]. Specifically, if the starting point of the state process is far from the boundary, the exit probability decays sub-exponentially, and the high-order PCHIP interpolation compensates the accuracy loss near the boundary. Moreover, the proposed algorithm only needs one temporal loop to recover the full dynamics of exit probability, i.e.,  $P(t, x)$  for  $t \in \{0 = t_1 < t_2 < \dots < t_M = T_{\max}\}$ , and all propagation information only assemble once at each time step. The main features of the proposed method are summarized as follows:

- (a) The unconditional stability for any  $\Delta t$ , first-order convergence with respect to  $\Delta t$ , and second-order convergence with respect to  $\Delta x$ ;
- (b) The output of our method can be used to obtain the exit probability of the SDE with different initial conditions by doing simple convolution;
- (c) Recovering the entire dynamics of the exit probability  $P(t, x)$  by only one temporal

iteration, and easy implementation on GPUs.

To our knowledge, our method is the first one that possesses all the three features among existing methods for computing  $P(t, x)$ . In comparison, the MC methods have feature (c); the PDE solvers for the forward Fokker-Planck equations have feature (a), (c); the implicit PDE solvers for the backward (adjoint) Fokker-Planck equations have feature (a), (b); the explicit solvers for the backward (adjoint) Fokker-Planck equations have feature (b), (c).

The outline of the paper is as follows: In section 2, we introduce the formal definitions of exit time and exit probability. Moreover, we give mathematical descriptions of the stochastic dynamical system and the adjoint equation. In section 3, the fully-discrete probabilistic scheme and the determination of spatial discretization are given. In section 3.2, we provide an efficient implementation for computing the full dynamics of exit probability. Practical numerical examples are given in section 4, which are consistent with theoretical results. Some conclusions are shown in section 5.

## 2. Problem setting

Our starting point is the  $d$ -dimensional stochastic differential equation

$$X_t = X_0 + \int_0^t b(s, X_s)ds + \int_0^t \sigma(s, X_s)dW_s \quad \text{with } X_0 \in \mathcal{D} \subset \mathbb{R}^d, \quad (1)$$

where  $W_t := (W_t^1, \dots, W_t^m)^\top$  is an  $m$ -dimensional standard Brownian motion,  $X_t \in \mathbb{R}^d$ .  $b : [0, T_{\max}] \times \mathbb{R}^d \rightarrow \mathbb{R}^d$ ,  $\sigma : [0, T_{\max}] \times \mathbb{R}^d \rightarrow \mathbb{R}^{d \times m}$  are globally Lipschitz in  $x$  uniformly with respect with respect to  $t$ , and locally bounded. And  $X_0$  is an initial condition in an open bounded domain  $\mathcal{D} = (\alpha_1, \beta_1) \times \dots \times (\alpha_d, \beta_d) \subset \mathbb{R}^d$ . The first exit time,  $\tau$ , is defined as

$$\tau := \inf \{t > 0 \mid X_0 \in \mathcal{D}, X_t \notin \mathcal{D}\}, \quad (2)$$

which is the first time instant when  $X_t$  in Eq. (1) exits the domain  $\mathcal{D}$ .

Our objective is to numerically compute the *exit probability*,  $P(t, x)$ , defined as the probability of the event that the stochastic process in Eq. (1) exits the domain  $\mathcal{D}$  at or before a specific time  $t \in (0, T_{\max})$

$$P(t, x) = \mathbb{P} \{ \tau \leq t \mid X_0 = x \in \mathcal{D} \} \quad \text{for any } (t, x) \in [0, T_{\max}] \times \overline{\mathcal{D}}. \quad (3)$$

Note that  $P(t, x)$  in Eq. (3) is independent of the distribution,  $P_{\text{init}}(X_0)$ , of the initial condition,  $X_0$ . Once  $P(t, x)$  is computed, the exit probability conditional on an initial distribution  $P_{\text{init}}(X_0)$  is given by the convolution

$$\mathbb{P} \{ \tau \leq t \mid X_0 \sim P_{\text{init}}(X_0) \} = \int P(t, x) P_{\text{init}}(x) dx.$$

In this sense,  $P(t, x)$  in Eq. (3) can be viewed as a Green's function for the exit probability problem of interest. This feature can save significant computing effort when studying the dynamics of  $P(t, x)$  as function of different distributions of initial conditions as typically done in applied problems (e.g., the runaway electron acceleration problem in Section 4.3).

For a fixed  $T \in (0, T_{\max})$ , the exit probability  $P(T, x)$  in Eq. (3) can be obtained from

$$P(T, x) = u(0, x), \quad (4)$$

where  $u(t, x)$  is the solution of the parabolic terminal boundary value problem of the *backward (adjoint) Fokker-Planck equation* [34],

$$\begin{aligned} \frac{\partial u(t, x)}{\partial t} + \mathcal{L}^*(t, x)[u(t, x)] &= 0 \quad \text{for } x \in \mathcal{D}, t < T, \\ u(t, x) &= 1 \quad \text{for } x \in \partial\mathcal{D}, t < T, \\ u(T, x) &= 0 \quad \text{for } x \in \mathcal{D}, \end{aligned} \quad (5)$$

where the operator  $\mathcal{L}^*(t, x)$ , which is the adjoint of the forward Fokker-Planck operator associated with  $X_t$ , is given by

$$\mathcal{L}^*(t, x)[u] := \sum_{i=1}^d b_i(t, x) \frac{\partial u}{\partial x^i}(t, x) + \frac{1}{2} \sum_{i,j=1}^d (\sigma\sigma^\top)_{i,j} \frac{\partial^2 u}{\partial x^i \partial x^j}(t, x),$$

with  $b_i$  the  $i$ -th component of the drift  $b(t, x)$ ,  $(\sigma\sigma^\top)_{i,j}$  the  $(i, j)$ -th entry of the diffusivity tensor  $\sigma\sigma^\top$ , and  $x^i$  the  $i$ -th component of  $x$  in Eq. (1).

The full dynamics of  $P(t, x)$  for any  $(t, x) \in [0, T_{\max}] \times \mathcal{D}$  can then be approximated by solving Eq. (5)  $M$ -times for the terminal times

$$\mathcal{T} := \{0 = T_0 < T_1 < \dots < T_M = T_{\max}\}, \quad (6)$$

and then interpolating the solution outside the grid points. Although classical PDE solvers based on finite difference or finite element methods can be used to solve Eq. (5), these methods might be inefficient in approximating the entire dynamics of  $P(t, x)$  due to time stepping numerical stability issue. Using explicit time stepping methods allows to stack the  $M$  terminal value problems together in a matrix and push through explicit propagators. However, explicit schemes usually require small time step size to guarantee numerical stability. Implicit time stepping can guarantee stability. However, implicit methods require solving a linear system at each time step, such that multiple linear systems (e.g.,  $M$  linear systems at  $T_0$ ) need to be solved independently at each time step. As it will be discussed below, the proposed numerical method bypasses these difficulties by using an explicit yet *unconditionally stable* time stepping algorithm.

In applications of interest to plasma physics, as well as in other areas, the parameters in the SDEs, e.g.,  $\sigma$  and  $b$  in Eq (1), are determined from a self-consistent coupling to another mathematical model governing their evolution. Although incorporating this type of couplings using PDE methods is in principle possible, in practice it can be quite difficult and the proposed method can be used to overcome these challenges.

### 3. The proposed Feynman-Kac based numerical method

The theoretical foundation of our probabilistic method is the Feynman-Kac theory that links the SDE in Eq. (1) to the adjoint equation in Eq. (5), see for example Refs. [24, 46]. In Sec. 3.1 we focus on the computation of  $P(T, x)$  at a fixed time. In Sec. 3.2 we present an efficient algorithm to compute  $P(t, x)$  for  $t \in [0, T_{\max}]$  based on the simultaneous solution of  $M$  adjoint equations with  $M$  different terminal time instants.

#### 3.1. The numerical scheme for the exit probability at a fixed time

The first step is to write the probabilistic representation of the solution  $u(t, x)$  in Eq. (5). To this end, we rewrite the SDE in Eq. (1) in the conditional form

$$X_s^{t,x} = x + \int_t^s b(r, X_r^{t,x})dr + \int_t^s \sigma(r, X_r^{t,x})dW_r \quad \text{for } s \geq t, \quad (7)$$

where the superscript  $t,x$  indicates the condition that  $X_s^{t,x}$  starts from  $(t, x) \in [0, T_N] \times \mathcal{D}$ . Note that  $T_N$  is the  $N$ -th element of the set  $\mathcal{T}$  in Eq. (6). Accordingly, we can define the *first conditional exit time*

$$\tau_{t,x} := \inf\{s > t \mid x \in \mathcal{D}, X_s^{t,x} \notin \mathcal{D}\}. \quad (8)$$

The probabilistic representation of  $u(t, x)$  in Eq. (5) is given by the Feynman-Kac formula [23, 16]

$$u(t, x) = \mathbb{E} \left[ u \left( s \wedge \tau_{t,x}, X_{s \wedge \tau_{t,x}}^{t,x} \right) \right], \quad (9)$$

where  $s \wedge \tau_{t,x} := \min(s, \tau_{t,x})$  denotes the minimum of  $\tau_{t,x}$  and  $s$  and  $X_{s \wedge \tau_{t,x}}^{t,x}$  is defined based on Eq. (7). Instead of solving the PDE in Eq. (5), our approach is based on the direct computation of  $u(t, x)$  by discretizing Eq. (9). The temporal and spatial approximations used to accomplish this are introduced in Section 3.1.1 and Section 3.1.2, respectively. The estimation of the mathematical expectation  $\mathbb{E}[\cdot]$  is introduced in Section 3.1.4.

##### 3.1.1. Temporal approximation of $u(t, x)$

We introduce a uniform time partition for  $[0, T_N]$ :

$$\mathcal{T}_N := \{0 = t_0 < t_1 < \dots < t_N = T\} \quad (10)$$

with  $\Delta t = t_{n+1} - t_n$  for  $n = 0, 1, \dots, N$ . We assume  $\mathcal{T}_N$  is a subset of  $\mathcal{T}$  in Eq. (6), which means  $t_n = T_n$  for  $n = 0, \dots, N$ . We discretize the SDE in Eq. (7) in the interval  $[t_n, t_{n+1}]$  using a forward Euler scheme [48, 29]:

$$X_{n+1}^{t_n, x} = x + b(t_n, x)\Delta t + \sigma(t_n, x)\Delta W, \quad (11)$$

where  $\Delta W = W_{t_{n+1}} - W_{t_n}$ . Substituting Eq. (11) into Eq. (9), we approximate the solution of  $u(t, x)$  at  $t = t_n$  using

$$u(t_n, x) \approx u^n(x) = \mathbb{E} \left[ u^{n+1} \left( X_{n+1}^{t_n, x} \right) \mathbf{1}_{\{\tau_{t_n, x} > t_{n+1}\}} \right] + \mathbb{P}(\tau_{t_n, x} \leq t_{n+1}), \quad (12)$$

where  $\tau_{t_n, x}$  is defined in Eq. (8)<sup>1</sup>,  $\mathbf{1}_{\{\tau_{t_n, x} > t_{n+1}\}}$  is the indicator function of the event that  $X_s^{t_n, x}$  does not exit from  $\mathcal{D}$  before  $t_{n+1}$ , and  $\mathbb{P}(\tau_{t_n, x} \leq t_{n+1})$  is the probability that  $X_s^{t_n, x}$  exits from  $\mathcal{D}$  within  $(t_n, t_{n+1}]$ .

### 3.1.2. Spatial approximation of $u(t, x)$

To approximate  $u^n(x)$  in  $\mathcal{D}$  we use piecewise polynomial interpolation. We first introduce a Cartesian mesh  $\mathcal{S} = \mathcal{S}^1 \times \mathcal{S}^2 \times \cdots \times \mathcal{S}^d$  for the domain  $\overline{\mathcal{D}}$ , where  $\mathcal{S}^i$  for  $i = 1, \dots, d$  is a mesh of the interval  $[\alpha_i, \beta_i]$ . It should be noted that the partition along each direction may be non-uniform. For notational simplicity, we use  $J$  to denote the total number of grid points in  $\mathcal{S}$ , and use a scalar  $j$  to index all the grid points in  $\mathcal{S}$ , i.e.,

$$\mathcal{S} := \{x_j : j = 1, \dots, J\}.$$

The general formula for piecewise interpolation using nodal values can be written as

$$u^{n, J}(x) := \sum_{j=1}^J u_j^n \psi_j(x) + \langle \mathbf{d}u_j^n, \Phi_j(x) \rangle, \quad \text{for } x \in \overline{\mathcal{D}}, \quad (13)$$

where  $u_j^n$  for  $j = 1, \dots, J$  are the approximate nodal values of  $u(t_n, x)$ ,  $\mathbf{d}u_j^n$  for  $j = 1, \dots, J$  are gradient at nodal  $x_j$ .  $\psi_j(x), \Phi_j(x)$  are generated by assembly all the basis functions associated with the  $j$ -th nodal value  $u_j^n$  and  $\mathbf{d}u_j^n$ . Since  $u(t, x)$  is a probability taking values within  $[0, 1]$ , we use the Piecewise Cubic Hermite Interpolating Polynomials (PCHIP) [17] to implement Eq. (13). A brief description of the used interpolation scheme is given below.

*Piecewise cubic Hermite interpolating polynomials.* For simplicity, we briefly recall the one-dimensional PCHIP interpolation. Since we are using a Cartesian grid, the one-dimensional scheme can be easily extended to multi-dimensional grid by tensor product [21]. Taking  $[x_j, x_{j+1}]$  as an example, the PCHIP approximation of  $u^n(x)$  in  $[x_j, x_{j+1}]$  can be written as

$$\begin{aligned} u^{n, J}(x) = & \frac{3hs^2 - 2s^3}{h^3} u_{j+1}^n + \frac{h^3 - 3hs^2 + 2s^3}{h^3} u_j^n \\ & + \frac{s^2(s-h)}{h^2} \frac{du^n}{dx}(x_{j+1}) + \frac{s(s-h)^2}{h^2} \frac{du^n}{dx}(x_j), \end{aligned} \quad (14)$$

where  $s = x - x_j$  and  $h = x_{j+1} - x_j$ . As the derivatives  $\frac{du^n}{dx}(x_{j+1})$  and  $\frac{du^n}{dx}(x_j)$  are unavailable, approximated derivatives are used instead. When  $x_j$  is an interior node,  $\frac{du^n}{dx}(x_j)$  is approximated by

$$\frac{du^n}{dx}(x_j) = \begin{cases} 0 & \text{if } \delta_j \text{ and } \delta_{j-1} \text{ have opposite signs,} \\ \frac{2}{\frac{1}{\delta_{j-1}} + \frac{1}{\delta_j}} & \text{if } \delta_j \text{ and } \delta_{j-1} \text{ have same sign,} \end{cases} \quad (15)$$

---

<sup>1</sup>The exit time  $\tau_{t_n, x}$  in Eq. (8) should be defined by replacing  $X_s^{t_n, x}$  with the Euler discretization, i.e.,  $X_s^{t_n, x} = x + b(t_n, x)(s - t_n) + \sigma(t_n, x)(W_s - W_{t_n})$  for  $s \geq t_n$  in Eq. (8). We use the same notation without creating confusion.



where  $\delta_j$  is the first divided difference given by  $\delta_j = \frac{u_{j+1}^n - u_j^n}{x_{j+1} - x_j}$ . For the boundary node  $x_1$ ,  $\frac{du^n}{dx}(x_1)$  is defined by substituting  $\delta_1$  and  $\delta_2$  into Eq. (15); for the boundary node  $x_J$ ,  $\frac{du^n}{dx}(x_J)$  is defined by substituting  $\delta_{J-1}$  and  $\delta_{J-2}$  into Eq. (15).

### 3.1.3. Treatment of the probability $\mathbb{P}(\tau_{t_n,x} \leq t_{n+1})$

$\mathbb{P}(\tau_{t_n,x} \leq t_{n+1})$  in Eq. (12) describes the probability that  $X_s^{t_n,x}$  exits from  $\mathcal{D}$  within  $(t_n, t_{n+1}]$ . It is challenging to approximate the probability with high-order accuracy for any  $x$  in  $\mathcal{D}$ . In our method, we only need to deal with  $\mathbb{P}(\tau_{t_n,x} \leq t_{n+1})$  with  $x$  being the interior nodes of the spatial mesh  $\mathcal{S}$ . Thus, our idea is to impose an additional condition on  $\mathcal{S}$  to guarantee that  $\mathbb{P}(\tau_{t_n,x} \leq t_{n+1})$  is sufficiently small, e.g., on the order of the temporal or spatial approximation errors.

It is known that  $\mathbb{P}(\tau_{t_n,x} \leq t_{n+1}) \rightarrow 1$  as  $x \rightarrow \partial\mathcal{D}$ . In our previous work [41], we proved that if  $b$  and  $\sigma$  are bounded functions, i.e.,  $|b(t, x)| \leq \bar{b}$  and  $|\sigma(t, x)| \leq \bar{\sigma}$  for  $(t, x) \in [0, T_{\max}] \times \mathcal{D}$  with  $0 \leq \bar{b}, \bar{\sigma} \leq +\infty$ , and  $x$  in Eq. (11) is sufficiently far from the boundary  $\partial\mathcal{D}$  satisfying  $\text{dist}(x, \partial\mathcal{D}) \sim \mathcal{O}((\Delta t)^{1/2-\varepsilon})$  for any given constant  $\varepsilon > 0$ , then for sufficiently small  $\Delta t$ , it holds that

$$\mathbb{P}(\tau_{t_n,x} \leq t_{n+1}) \leq C(\Delta t)^\varepsilon \exp\left(-\frac{1}{(\Delta t)^{2\varepsilon}}\right), \quad (16)$$

where the constant  $C > 0$  only depends on upper constants  $\bar{b}, \bar{\sigma}$ . Even though the estimate in Eq. (16) was proved in [41] for the one-dimensional case, it provides a good insight to deal with  $\mathbb{P}(\tau_{t_n,x} \leq t_{n+1})$ . Specifically, we impose the following assumption on the spatial mesh  $\mathcal{S}$ .

**Assumption 1.** For any interior node  $x_j \in \mathcal{S} \cap \mathcal{D}$ , it holds that

$$\text{dist}(x_j, \partial\mathcal{D}) \geq C\sqrt{\Delta t}, \quad (17)$$

where the constant  $C > 0$  only depends on upper constants  $\bar{b}, \bar{\sigma}$ ,  $\text{dist}(x_j, \partial\mathcal{D})$  is the smallest Euclidean distance between  $x_j$  and  $\partial\mathcal{D}$  for  $x_j \in \mathcal{S} \cap \mathcal{D}$ .

Note that this assumption is much weaker than a condition on the maximum spatial mesh size, because it only applies to the closest layer of the interior nodes to the boundary. In other words, it provides sufficient flexibility to use non-uniform spatial meshes to handle irregular behaviors (e.g., the sharp transition layer of the RE problem in Section 4.3). How to realize Assumption 1 in practice will be discussed in Remark 2.

When  $\mathcal{S}$  satisfies Assumption 1, the probability  $\mathbb{P}(\tau_{t_n,x} \leq t_{n+1}) = 1 - \mathbb{P}(\tau_{t_n,x} > t_{n+1})$  is very close to zero, which implies that

$$|\mathbb{E}[u^{n+1}(X_{n+1}^{t_n,x})] - \mathbb{E}[u^{n+1}(X_{n+1}^{t_n,x}) \mathbf{1}_{\{\tau_{t_n,x} > t_{n+1}\}}]| \sim \mathcal{O}(\mathbb{P}(\tau_{t_n,x} \leq t_{n+1})),$$

because  $u^{n+1}$  takes values from  $[0, 1]$ . This means the indicator function  $\mathbf{1}_{\{\tau_{t_n,x} > t_{n+1}\}}$  approaches 1 in Eq. (12). Hence, by substituting the spatial approximation  $u^{n,J}, u^{n+1,J}$  into Eq. (12) and imposing Assumption 1 on  $\mathcal{S}$ , Eq. (12) reduces to

$$u_j^n = \mathbb{E}[u^{n+1,J}(X_{n+1}^{t_n,x_j})] \quad \text{for } x_j \in \mathcal{S} \cap \mathcal{D}, \quad (18)$$

and  $u^{n,J}(x)$  can be obtained by interpolating the nodal values  $u_j^n$  using Eq. (13).



### 3.1.4. Quadrature for the conditional expectation

The last piece of the algorithm is a quadrature rule for estimating the conditional expectations for the interior nodes  $x_j \in \mathcal{S} \cap \mathcal{D}$  given by the  $d$ -dimensional integrals

$$\mathbb{E}[u^{n+1,J}(X_{n+1}^{t_n, x_j})] = \int_{\mathbb{R}^d} u^{n+1,J}(x_j + b(t_n, x_j)\Delta t + \sigma(t_n, x_j)\sqrt{2\Delta t}\xi) \rho(\xi) d\xi, \quad (19)$$

where  $\xi := (\xi_1, \dots, \xi_d)$  follows the normal distribution with density  $\rho(\xi) := \pi^{-d/2} \exp(-\sum_{\ell=1}^d \xi_\ell^2)$ . We use tensor-product Gauss-Hermite quadrature rule to approximate Eq. (19). Denoting by  $\{w_q\}_{q=1}^Q$  and  $\{a_q\}_{q=1}^Q$  the weights and abscissae of the  $Q$ -point tensor-product Gauss-Hermite rule, the approximation, denoted by  $\widehat{\mathbb{E}}[\cdot]$  is given by

$$\widehat{\mathbb{E}}[u^{n+1,J}(X_{n+1}^{t_n, x_j})] = \sum_{q=1}^Q w_q u^{n+1,J}(z_{jq}^n) \quad (20)$$

where

$$z_{jq}^n := x_j + b(t_n, x_j)\Delta t + \sigma(t_n, x_j)\sqrt{2\Delta t} a_q. \quad (21)$$

Substituting Eq. (20) into Eq. (18), completes our numerical scheme for approximating the nodal value

$$u_j^n = \widehat{\mathbb{E}}[u^{n+1,J}(X_{n+1}^{t_n, x_j})], \quad \text{for } x_j \in \mathcal{S} \cap \mathcal{D}, \quad (22)$$

from where  $u^{n,J}(x)$  can be obtained by interpolating  $u_j^n$  using Eq. (13).

**Remark 1.** Let  $Q^* = Q^{1/d}$  denote the number of quadrature points in each dimension. If  $u^{n+1,J}(\cdot)$  is sufficiently smooth, i.e.,  $\partial^{2J^*} u^{n+1,J} / \partial \xi_\ell^{2Q^*}$  is bounded for  $\ell = 1, \dots, d$ , then the quadrature error is bounded by [30]

$$\left| \widehat{\mathbb{E}}[u^{n+1,J}(X_{n+1}^{t_n, x_j})] - \mathbb{E}[u^{n+1,J}(X_{n+1}^{t_n, x_j})] \right| \leq C \frac{Q^*!}{2^{Q^*}(2Q^*)!} (\Delta t)^{Q^*},$$

where the constant  $C$  is independent of  $Q^*$  and  $\Delta t$ . Note that the factor  $(\Delta t)^{Q^*}$  comes from the  $2Q^*$ -th order differentiation of the function  $u^{n+1,J}$  with respect to  $\xi_\ell$  for  $\ell = 1, \dots, d$ . Therefore, to achieve  $\mathcal{O}(\Delta t)$  convergence only  $Q^* = 3$  quadrature points in each dimension are needed.

**Remark 2.** Since only a finite number of quadrature points are needed to approximate  $\mathbb{E}[\cdot]$ , Assumption 1 is satisfied by generating a spatial mesh  $\mathcal{S}$  such that all the quadrature points  $z_{jq}^n$  defined in Eq. (21) for  $x_j \in \mathcal{S} \cap \mathcal{D}$ ,  $q = 1, \dots, Q$  are located in  $\overline{\mathcal{D}}$ .

Summarizing, the proposed fully-discrete probabilistic scheme for the backward adjoint equation in Eq. (5) for a fixed terminal time  $T_N \in \mathcal{T}$  consists of the following steps:

**Scheme 1 (The backward scheme for the adjoint equation).** Given the temporal spatial partition  $\mathcal{T}_N \times \mathcal{S}$ , the terminal condition  $u^N(x_j)$  for  $x_j \in \mathcal{S}$ , and the boundary condition  $u^n(x_j)$  for  $x_j \in \mathcal{S} \cap \partial\mathcal{D}$ . For  $n = N - 1, \dots, 0$ , the approximation of  $u(t_n, x)$  is constructed via the following steps:

- *Step 1: generate quadrature abscissae  $\{z_{jq}^n\}_{q=1}^Q$  via Eq. (21), for  $x_j \in \mathcal{S} \cap \mathcal{D}$ ;*
- *Step 2: interpolate  $u^{n+1,J}(x)$  at the quadrature abscissae to obtain  $\{u^{n+1,J}(z_{jq}^n)\}_{q=1}^Q$ ;*
- *Step 3: compute the nodal values  $u_j^{n,J}$  using the quadrature rule in Eq. (22);*
- *Step 4: construct the interpolant  $u^{n,J}(x)$  by substituting  $\{u_j^{n,J}\}_{j=1}^J$  into Eq. (13).*

There is no stability condition, e.g., the CFL condition for the explicit finite difference method, forced on Scheme 1. Given a fixed spatial mesh  $\mathcal{S}$ , our method is stable with any  $\Delta t$ . As Fig. 1 shown, when Assumption 1 failed, the error does not decay in the order of  $\mathcal{O}(\Delta t)$ , but it does not blow up neither. Moreover, the error of Scheme 1:  $e_n = |u(t_n, x) - u^{n,J}(x)|$  is controlled by

$$e_n \sim \mathcal{O}\left(\Delta t + \frac{(\Delta x)^{p+1}}{\Delta t}\right), \quad (23)$$

where  $\Delta x := \max_{i \in \mathcal{S} \cap \mathcal{D}} \Delta x_i$ . The proof of the error estimate is out of the scope of this paper, the reader refer to works [47, 49] for details. In addition, since all grid points  $x_i$  are sufficiently far from the boundary  $\partial\mathcal{D}$ , i.e.,  $\Delta x$  is on the order of  $(\Delta t)^{\frac{1}{2}}$ , the use of PICHIP interpolation method ( $p = 3$ ) can provide sufficient accuracy near the boundary. Hence, our method achieves first order convergence in  $\Delta t$  and second order convergence in  $\Delta x$ .

### 3.2. Extension of Scheme 1 to computing the exit probability in $[0, T_{\max}]$

Scheme 1 provides an efficient and accurate method to solve the adjoint equation in Eq. (5) for a fixed  $T_N \in \mathcal{T}$ , which gives the approximation of the exit probability  $P(T_N, x) = u(0, x)$  at one time instant. A naive strategy to obtain the full dynamics of  $P(t, x)$  for  $(t, x) \in \mathcal{T} \times \mathcal{S}$  would be to repeatedly solve the adjoint equation in Eq. (5)  $M$  times. Although straightforward, this approach is extremely inefficient. To address this issue, here we propose a novel strategy based on the explicit nature of the proposed probabilistic scheme.

As a first step, we rewrite the interpolation (Step 2 of Scheme 1) in matrix form

$$\mathbf{u}_{\text{quad}}^{n+1} = \Psi^n \begin{pmatrix} \mathbf{u}^{n+1} \\ \mathbf{d}\mathbf{u}^{n+1} \end{pmatrix} := \Psi^n \mathcal{F}^n \mathbf{u}^{n+1}, \quad (24)$$

where  $\mathcal{F}^n$  is the operation to obtain the vector  $[\mathbf{u}^{n+1}; \mathbf{d}\mathbf{u}^{n+1}]$ . And  $\mathbf{d}\mathbf{u}^{n+1}$  is a  $Jn \times 1$  matrix that contains all partial derivatives at all grid points, where  $n$  is the dimension.  $\mathbf{u}^{n+1}$ ,  $\mathbf{u}_{\text{quad}}^{n+1}$  and  $\Psi^n$  are  $J \times 1$ ,  $JQ \times 1$  and  $JQ \times (n+1)J$  matrices, respectively, i.e.,

$$\mathbf{u}^{n+1} := \begin{pmatrix} u_1^{n+1} \\ u_2^{n+1} \\ \vdots \\ u_J^{n+1} \end{pmatrix}, \quad \mathbf{u}_{\text{quad}}^{n+1} := \begin{pmatrix} u^{n+1,J}(z_{11}^n) \\ u^{n+1,J}(z_{12}^n) \\ \vdots \\ u^{n+1,J}(z_{jq}^n) \end{pmatrix},$$

$$\Psi^n := \begin{pmatrix} \psi_1(z_{11}^n) & \cdots & \psi_J(z_{11}^n) & \phi_{11}(z_{11}^n) & \cdots & \phi_{1J}(z_{11}^n) & \cdots & \phi_{n1}(z_{11}^n) & \cdots & \phi_{nJ}(z_{11}^n) \\ \psi_1(z_{12}^n) & \cdots & \psi_J(z_{12}^n) & \phi_{11}(z_{12}^n) & \cdots & \phi_{1J}(z_{12}^n) & \cdots & \phi_{n1}(z_{11}^n) & \cdots & \phi_{nJ}(z_{11}^n) \\ \vdots & & \vdots & \vdots & \vdots & \vdots & & \vdots & & \vdots \\ \psi_1(z_{MJ}^n) & \cdots & \psi_J(z_{jq}^n) & \phi_{11}(z_{MJ}^n) & \cdots & \phi_{1J}(z_{jq}^n) & \cdots & \phi_{n1}(z_{11}^n) & \cdots & \phi_{nJ}(z_{11}^n) \end{pmatrix},$$

basis for  $u^{n+1}$ 
basis for  $du^{n+1}/dx_1$ 
basis for  $du^{n+1}/dx_n$

and  $\{z_{jq}^n\}$  is defined in Eq. (21).

Similarly, we rewrite the quadrature (Step 3 in Scheme 1) in matrix form

$$\mathbf{u}^n = \mathbf{Q} \mathbf{u}_{\text{quad}}^{n+1}, \quad (25)$$

where  $\mathbf{u}^n$  and  $\mathbf{Q}$  are  $J \times 1$  and  $J \times JQ$  matrices, respectively, i.e.,

$$\mathbf{n}^n := \begin{pmatrix} u_1^n \\ u_2^n \\ \vdots \\ u_J^n \end{pmatrix}, \quad \mathbf{Q} := \begin{pmatrix} w_1 & \cdots & w_Q & & & \\ & & & w_1 & \cdots & w_Q \\ & & & & \ddots & \\ & & & & & w_1 & \cdots & w_Q \end{pmatrix}. \quad (26)$$

In this notation, the propagation from  $\mathbf{u}^{n+1}$  to  $\mathbf{u}^n$  is represented by

$$\mathbf{u}^n = \mathbf{Q} \Psi^n \mathcal{F}^n \mathbf{u}^{n+1}. \quad (27)$$

By defining the terminal condition as

$$\chi(x) := \begin{cases} 0, & x \in \mathcal{D}, \\ 1, & x \in \partial\mathcal{D}, \end{cases} \quad (28)$$

the exit probability  $P(t, x)$  for a fixed  $t_n \in \mathcal{T}$  can be approximated by

$$\mathbf{p}^n = \mathbf{Q} \Psi^0 \mathcal{F}^0 (\mathbf{Q} \Psi^1 \mathcal{F}^1 \cdots (\mathbf{Q} \Psi^{n-1} \mathcal{F}^{n-1} \chi)), \quad (29)$$

where  $\mathbf{p}^n := (p_1^n, \dots, p_J^n)^\top \approx (P(t_n, x_1), \dots, P(t_n, x_J))$  and  $\chi := (\chi(x_1), \dots, \chi(x_J))$ . As aforementioned, the naive way to compute  $\mathbf{p}^n$  is to run the recursive form in Eq. (29)  $M$  times for  $n = 0, \dots, M-1$ , which requires either storing all the  $\Psi^n$  or re-assembling  $\Psi^n$  for  $n$  times. Since the assembling of  $\Psi^n$  requires interpolation on the spatial mesh  $\mathcal{S}$ , such strategy becomes very inefficient as the degrees of freedom  $M$  increases. To address this issue, we developed the following algorithm that only assembles  $\Psi^n$  once as well as does not need to store the generated  $\Psi^n$  for the following time steps.

---

**Algorithm 1**

- 1: **Initialization:**  $\mathbf{P} = \text{zeros}(J, M)$ ,  $\boldsymbol{\chi} = (\chi(x_1), \dots, \chi(x_J))^\top$ ;
  - 2: Generate the matrix  $\mathbf{Q}$  in Eq. (26);
  - 3: Evaluate  $\mathbf{P}(1 : J, 1 : M) = \text{repmat}(\boldsymbol{\chi}, 1, M)$ ;
  - 4: **For**  $n = M, \dots, 1$
  - 5:     Generate the interpolation matrix  $\boldsymbol{\Psi}^{n-1}$  in Eq. (24);
  - 6:     Generate the value matrix  $\mathcal{F}^{n-1}\mathbf{P}(1 : J, n : M)$  in Eq. (24);
  - 7:     Update  $\mathbf{P}(1 : J, n : M) = \mathbf{Q}\boldsymbol{\Psi}^{n-1} \mathcal{F}^{n-1}\mathbf{P}(1 : J, n : M)$ ;
  - 8: **End**
  - 9: **Output:**  $\mathbf{P}(1 : J, 1 : M)$ ;
- 

The  $n$ -th column of the output  $\mathbf{P}$  is the approximation of the exit probability  $P(t, x)$  at the time step  $t_n \in \mathcal{T}$  on the spatial mesh  $\mathcal{S}$ .

### 3.2.1. GPU acceleration

The main computational burden in Algorithm 1 is the matrix-matrix production for updating the matrix  $\mathbf{P}$ . At each time step, we can directly assemble the product  $\mathbf{Q}\boldsymbol{\Psi}^n$ . Due to the local support of the basis functions  $\psi_j(x)$ , the product, it is easy to see that  $\mathbf{Q}\boldsymbol{\Psi}^n$  is a sparse matrix. By construction, the functions  $\psi_j(x)$  can be evaluated in  $\mathcal{O}(1)$  complexity, hence forming  $\mathbf{Q}\boldsymbol{\Psi}^n$  has the complexity  $\mathcal{O}(J \times Z)$  where  $Z$  is the number of non-zeros on each column. In contrast, the complexity of the matrix-matrix multiplication is  $\mathcal{O}(J^2 \times Z)$ , which dominates the total cost.

In this work, we utilized the GPU architecture to accelerate the computation for updating  $\mathbf{P}$ . The vendor provided GPU sparse linear algebra library (cuSparse) [22] provides two sparse matrix-matrix functions, where the sparse matrix has to be stored in row compressed format, the dense input matrix can be given in either row or column major format, and the result is always given in column major form. In addition, the sparse matrix has to be on the left. The formulation for updating  $\mathbf{P}$  in Algorithm 1 is very well suited for the cuSparse library. We implemented the GPU-enabled probabilistic scheme by coupling our code with the GPU version of the function approximation library TASMANIAN [37]. TASMANIAN provides acceleration via a set of custom CUDA kernels, while the performance of each kernel falls behind the vendor optimized library, the memory footprint is significantly lower since the matrix returned by the kernel has the correct format. The custom CUDA kernels provide a good compromise between performance and memory footprint.

## 4. Numerical examples

In this section we present three numerical examples illustrating and testing the proposed numerical method. The first example considers the computation of the exit time probability in a standard 1D Brownian motion. Since in this case the analytical expression of the exit probability is known, this example is used to demonstrate the convergence of our approach

and the efficiency of the GPU-accelerated algorithm. The second example considers the exit time in a 2D advection-diffusion problem with a time dependent incompressible fluid velocity field. This example is used to compare the stability, accuracy, and computational cost of our approach with the implicit and explicit finite different solution of the adjoint Fokker-Planck partial differential equation. The third example presents a 3D plasma physics motivated problem and illustrates the seamless incorporation of nonuniform spatial grids in our scheme.

#### 4.1. The 1D Brownian motion

In this case the dynamics is governed by the one-dimensional stochastic differential equation

$$X_t = X_0 + W_t \quad \text{with } X_0 \in [0, L] \subset \mathbb{R},$$

and  $t \in [0, T_{\max}]$ . According to Eq. (4), the exit time probability  $P(T, x)$  at  $T \leq T_{\max}$  is given by  $P(T, x) = u(t = 0, x)$  where  $u(t, x)$  is the solution of the terminal value problem

$$\begin{aligned} \frac{\partial u(t, x)}{\partial t} + \frac{1}{2} \frac{\partial^2 u(t, x)}{\partial x^2} &= 0 \quad \text{for } x \in [0, L], t < T, \\ u(t, x) &= 1 \quad \text{for } x = \{0, L\}, t < T, \\ u(T, x) &= 0 \quad \text{for } x \in [0, L]. \end{aligned} \tag{30}$$

From the known exact analytical solution of Eq. (30) it follows that

$$P(T, x) = 1 - \sum_{n=1}^{\infty} \frac{4}{n\pi} \sin\left(\frac{n\pi x}{L}\right) \exp\left[-\frac{1}{2} \left(\frac{n\pi}{L}\right)^2 T\right]. \tag{31}$$

Figure 1 shows the first-order convergence of our method with respect to  $\Delta t$  for the case  $L = 10$  and  $T_{\max} = 3$ , with the error given by the Frobenius norm of the difference of the numerically computed solution and the exact solution in Eq. (31). To balance the errors from quadrature and interpolation, we use 3-point Gauss-Hermite rule and enforce the condition on the spatial mesh  $\mathcal{S}$  which is discussed in Assumption 1 and Remark 2. In comparison, when replacing PCHIP interpolation with linear interpolation, the error decays slower, due to the enforcement of the condition  $\text{dist}(x_j, \partial\mathcal{D}) \geq C\sqrt{\Delta t}$  in Eq. (17) near the boundary  $\partial\mathcal{D}$ . On the other hand, when the condition in Eq. (17) is violated, i.e. when  $\text{dist}(x_j, \partial\mathcal{D}) < C\sqrt{\Delta t}$ , the error also decays slower because the probability  $\mathbb{P}(\tau_{t_n, x} \leq t_{n+1})$  is too big to be neglected for the grid points near  $\partial\mathcal{D}$ .

Figure 2 illustrates the GPU acceleration of Algorithm 1. For comparison we implemented both a CPU and GPU version in Matlab, and utilized a Matlab interface to call the GPU-based matrix-matrix multiplication module in TASMANIAN. The results were generated on a workstation with Intel Xeon W-2225 CPU and Nvidia Quadro P1000 GPU. The time reported in Figure 2 is the wall clock time for solving the entire problem. It is observed that the GPU-accelerated algorithm reduces the total computing time by up to 95%.

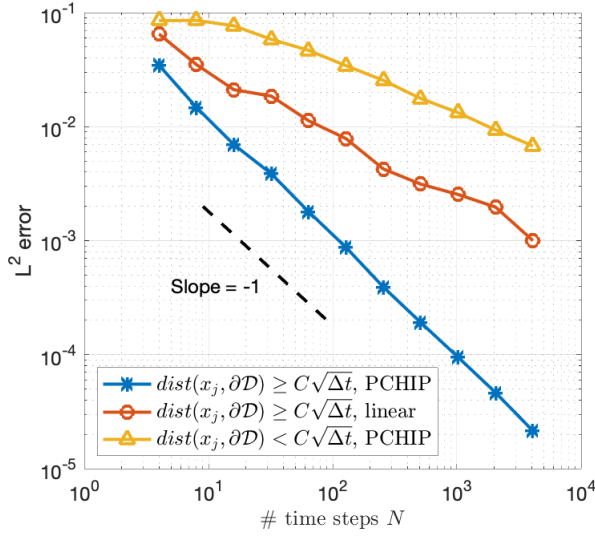


Figure 1: Error decay in the computation of  $P(T_{\max}, x)$ , for  $T_{\max} = 3$  and  $L = 10$ . The proposed method achieves  $\mathcal{O}(\Delta t)$  convergence when using 3-point Gauss-Hermite rule, PCHIP interpolation and enforcing  $\text{dist}(x_j, \partial\mathcal{D}) \geq C\sqrt{\Delta t}$  in Eq. (17) for  $x_j \in \mathcal{S} \cap \mathcal{D}$ . In comparison, the use of linear interpolation cannot provide sufficient accuracy near the boundary  $\partial\mathcal{D}$ ; violating the condition in Eq. (17) makes the probability  $\mathbb{P}(\tau_{t_n, x} \leq t_{n+1})$  is too big to be neglected for the grid points near  $\partial\mathcal{D}$ .

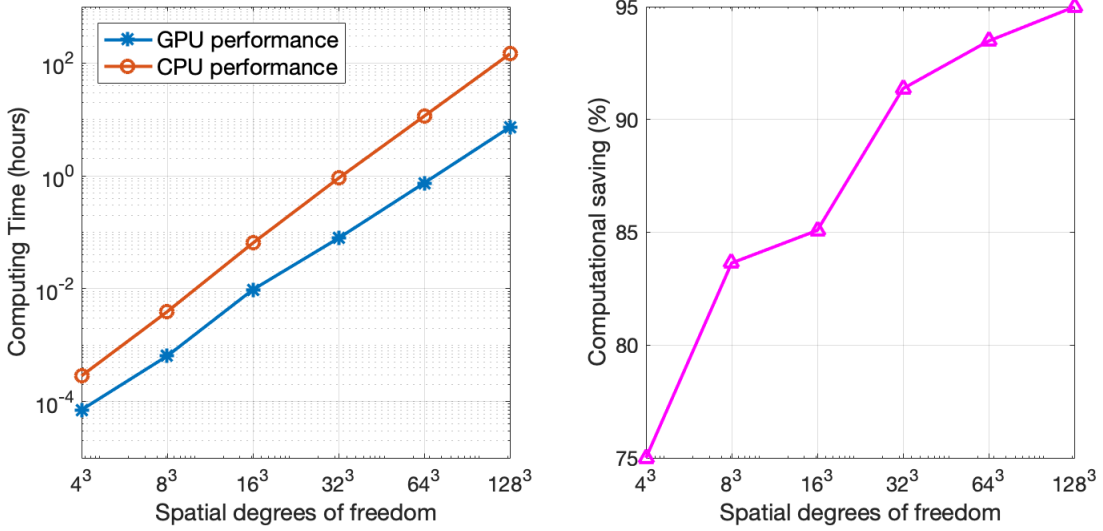


Figure 2: Performance comparison of GPU and CPU implementation of Algorithm 1 of the proposed method for the exit time probability in a 1D Brownian motion.

#### 4.2. A 2D advection diffusion problem

In this example we consider the transport of a scalar field  $u$  modeled by the advection-diffusion equation

$$\frac{\partial u(t, \mathbf{x})}{\partial t} + P_e \mathbf{v} \cdot \nabla u(t, \mathbf{x}) = \frac{1}{2} \nabla^2 u(t, \mathbf{x}), \quad (32)$$

for  $t \in [0, T_{max}]$  in the 2D domain  $\mathbf{x} \in \mathcal{D} := [-\pi, \pi] \times [0, L]$ , with time-dependent incompressible velocity field  $\mathbf{v} = v_{x_1} \mathbf{e}_{x_1} + v_{x_2} \mathbf{e}_{x_2}$ , where

$$v_{x_1} = -\pi \cos(\pi x_2) [\sin(nx_1) + \epsilon f(t) \cos(nx_1)], \quad (33)$$

$$v_{x_2} = n \sin(\pi x_2) [\cos(nx_1) - \epsilon f(t) \sin(nx_1)], \quad (34)$$

$$f(t) = \cos(\omega t). \quad (35)$$

This cellular flow velocity field [10] is a commonly used model to study transport in Rayleigh-Bernard convection, see e.g. [44]. The corresponding 2D, non-autonomous SDE system is

$$\begin{cases} dx_1 = P_e v_{x_1}(x_1, x_2, t) dt + dW_1, \\ dx_2 = P_e v_{x_2}(x_1, x_2, t) dt + dW_2, \end{cases} \quad (36)$$

where  $dW_1$  and  $dW_2$  are independent Wiener processes (Brownian motions).

We use dimensionless variables with  $\mathbf{x}$  normalized using the length scale  $L$ , and  $t$  normalized using the diffusion time scale  $T = L^2/D$ , where  $D$  is the diffusivity. The Péclet number  $P_e$  is defined as  $P_e = VL/D$  where  $V$  is the velocity scale. The free parameters of the model are  $P_e$ ,  $\epsilon$ ,  $\omega$ , and  $n$ . The regimen  $P_e \gg 1$  ( $P_e \ll 1$ ) corresponds to an advection (diffusion) dominated regime. On the other hand, the limit  $\omega \ll 1$  ( $\omega \gg 1$ ) corresponds to a perturbation with a period significantly longer (shorter) than the diffusion time scale. The parameter  $\epsilon$  determines the size of the perturbation and the number of cells in the flow pattern is  $2n$ . For the numerical simulations we take:  $P_e = 10$ ,  $\epsilon = 0.15$ ,  $\omega = 2\pi/10$ ,  $n = 2$ ,  $T_{max} = 0.05$ , and  $L = 1$ . The boundary conditions are periodic in  $x_1$ , and Dirichlet,  $P(t, x_1, 0) = P(t, x_1, 1) = 1$ , in  $x_2$ .

In this fluid mechanics problem the exit time probability corresponds to the probability that a Lagrangian element of the passive tracer  $u$  located at  $\mathbf{x}$  reaches the top ( $x_2 = 1$ ) or the bottom ( $x_2 = 0$ ) boundary. Since  $n = 2$ , in this case the unperturbed,  $\epsilon = 0$ , flow exhibits four convection rolls with centers at the stagnation elliptic points of the flow field located at  $(x_1, x_2) = (\pm\pi/4, 1/2)$  and  $(x_1, x_2) = (\pm 3\pi/4, 1/2)$ . The cells of the convection rolls are flanked by the vertical separatrices joining the hyperbolic stagnation points of the flow located at  $(x_1, x_2) = (\pm\pi/2, 0)$ ,  $(x_1, x_2) = (\pi, 0)$  and  $(x_1, x_2) = (0, 0)$  with those located at  $(x_1, x_2) = (\pm\pi/2, 1)$ ,  $(x_1, x_2) = (\pm\pi, 1)$  and  $(x_1, x_2) = (0, 1)$ . In the absence of a time dependent perturbation,  $\epsilon = 0$ , the migration towards the  $x_2 = 0$  and  $x_2 = 1$  boundaries is due to diffusion. However, when  $\epsilon \neq 0$  the flow field exhibits chaotic advection [1, 35] and transport is enhanced specially near the separatrices of the flow. This phenomenology is in agreement by the computed exit time probability shown in Fig. 3. In particular, the exit time probability is small in the vicinity of the elliptic points of the flow (i.e., the core of the convection rolls) and large near the separatrices and the hyperbolic stagnation points.

Figure 4 presents a comparative study of the error decay as function of the grid resolution.



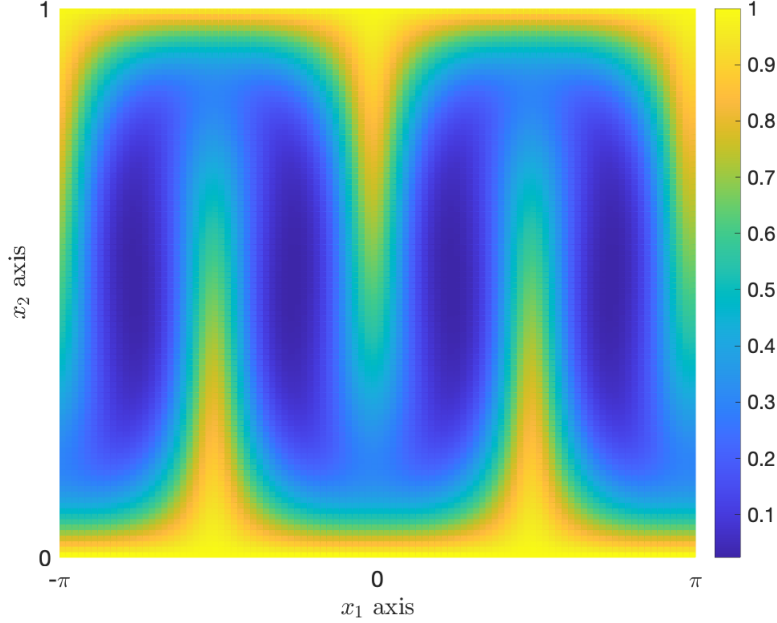


Figure 3: the exit probability  $P(\mathbf{x}, T_{\max})$  for the advection-diffusion problem in Eq. (32).

The error was quantified using the Frobenius norm of the difference of the computed solution and a reference solution. Since there are not known analytical solutions for this problem, we used as reference a high resolution numerical integration of Eq. (32) using an explicit finite difference (EFD) method. The reference solution was fully converged in the sense that it did not change when reducing the grid resolution and time step. As the left panel in Fig. 4 shows, our method achieves second-order convergence in  $\Delta \mathbf{x}$ , when Assumption 1 is satisfied. When Assumption 1 is not satisfied the error exhibits a slower decay but it does not blow up because the method is unconditionally stable. In contrast, as the middle panel shows, the implicit finite difference (IFD) method can only achieve first-order convergence in  $\Delta x$  provide a first-order upwind scheme is used to guarantee stability (the second-order central scheme is unstable). The EFD, shown in the right panel, can also exhibit first order convergence but it is significantly constrained by the CFL stability condition. The extension of first-order upwind schemes to higher order faces technical challenges at grid points adjacent to the boundary. For schemes using stencils involving values outside of the domain, there should be additional strategies to figure them out. In comparison, our method inherently simulates the direction of propagation of information, with the quadrature points incorporating the direction of advection.

Figure 5 compares the computational cost of the proposed method with the EFD and IFD methods. It is observed that, depending on the prescribed error, the new method requires up to several orders of magnitude less operations than finite difference methods for the computation of the full dynamics of the exit time probability in  $t \in [0, T_{\max}]$ . This is because our method only requires a single temporal iteration for computing the exit probability for all time instants in the interval  $[0, T_{\max}]$ . In contrast, the IFD scheme requires a double temporal iteration since it needs to solve the adjoint equation repeatedly to recover the full

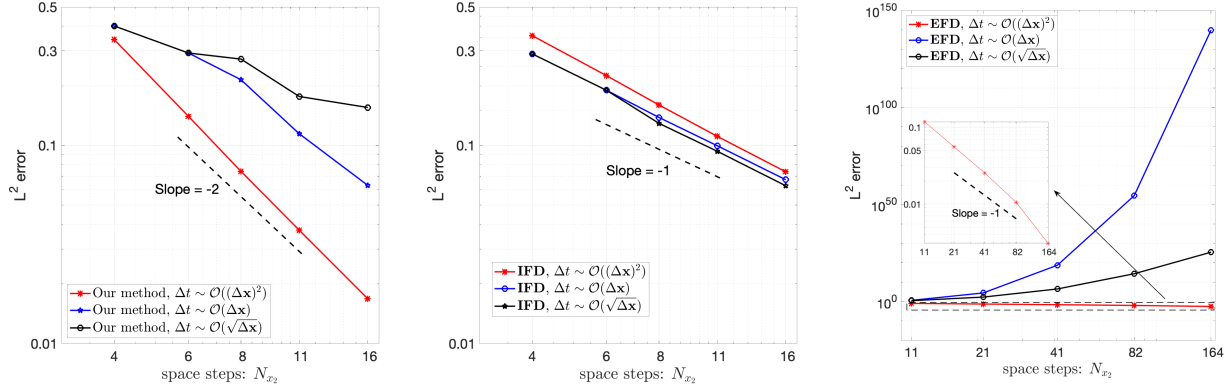


Figure 4: The proposed method is unconditional stable and exhibits second-order convergence in  $\Delta x$  when Assumption 1 is satisfied. In comparison, the implicit finite difference (IFD) and the explicitly finite difference (EFD) schemes exhibit first-order convergence. In addition, the EFD is constrained by the CFL condition to guarantee stability.

dynamics of the exit time probability. The EFD scheme is not much better due to the slow convergence rate,  $\sqrt{\Delta t} \sim \Delta x \sim \epsilon$ , and the need to satisfy the CFL condition.

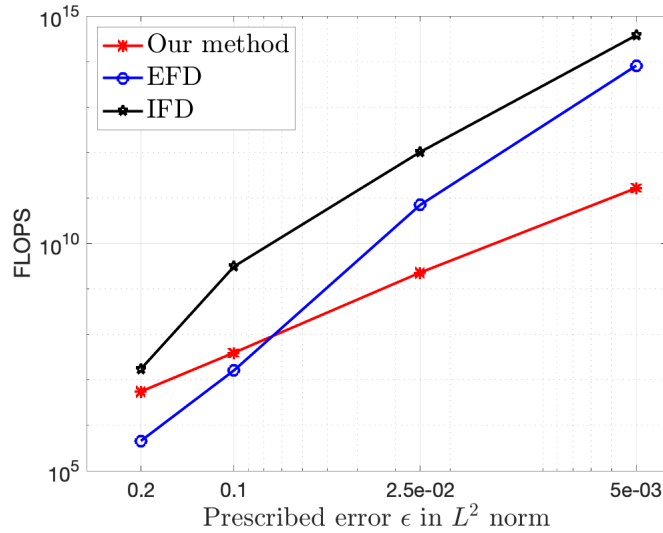


Figure 5: Comparison of the computational cost of the proposed method with EFD and IFD methods as function of the prescribed error. To achieve comparable small errors, EFD and IFD methods require several orders of magnitude more operations. This is because finite difference schemes require a double temporal iteration to recover the full dynamics of the exit probability. EFD are more efficient than IFD, but due to stability constraints, they require a large amount of time steps to achieve small errors.

#### 4.3. A 3D runaway electron problem

To demonstrate the seamless integration of the proposed method with nonuniform spatial grids, we consider a three-dimensional exit time probability problem motivated by plasma physics. The model of interest describes the acceleration of electrons in a magnetically confined plasma in a toroidal chamber (tokamak) in the presence of an electric field taking

into account collisional and radiation damping. The main physics problem is to understand the conditions under which the damping cannot overcome the electric field acceleration causing the electrons to “runaway” achieving arbitrarily large energies. Understanding this problem is critical for the safe operation of nuclear fusion reactors, because if these so-called runaway electrons (RE) are not avoided or controlled they can damage the plasma facing components of the reactor. This is a very complex problem, and here, as a proof-of-principle calculation, we consider a simplified model describing the evolution of the magnitude of the relativistic momentum of the electron, denoted by  $p$ , the cosine of the pitch angle,  $\xi = \cos \theta$ , where  $\theta$  is the angle between the momentum and the direction of the magnetic field used to confine the plasma, and the minor radius,  $r$ , of the toroidal confinement region. The time evolution of these variables is governed by the stochastic differential equations

$$\begin{cases} dp = \left[ E\xi - \frac{\gamma p}{\tau}(1 - \xi^2) - C_F(p) + \frac{1}{p^2} \frac{\partial}{\partial p} (p^2 C_A(p)) \right] dt + \sqrt{2C_A(p)} dW_p, \\ d\xi = \left[ \frac{E(1 - \xi^2)}{p} - \frac{\xi(1 - \xi^2)}{\tau\gamma} - 2\xi \frac{C_B(p)}{p^2} \right] dt + \frac{\sqrt{2C_B(p)}}{p} \sqrt{1 - \xi^2} dW_\xi, \\ dr = \left[ V(r) + \frac{\partial D(r, p)}{\partial r} \right] dt + \sqrt{2D(r, p)} dW_r. \end{cases} \quad (37)$$

where  $dW_p$ ,  $dW_\xi$  and  $dW_r$  are independent Wiener processes (standard Brownian motions),  $E$  is the electric field, and  $\tau$  the radiation damping time scale. The collision operator is determined by the functions  $C_A$ ,  $C_B$ , and  $C_F$  defined as

$$\begin{aligned} C_A(p) &= \bar{\nu}_{ee} \bar{v}_T^2 \frac{\psi(y)}{y}, \\ C_B(p) &= \frac{1}{2} \bar{\nu}_{ee} \bar{v}_T^2 \frac{1}{y} \left[ Z + \phi(y) - \psi(y) + \frac{y^2}{2} \delta^4 \right], \\ C_F(p) &= 2 \bar{\nu}_{ee} \bar{v}_T \psi(y), \\ \phi(y) &= \frac{2}{\sqrt{\pi}} \int_0^y e^{-s^2} ds, \quad \psi(y) = \frac{1}{2y^2} \left[ \phi(y) - y \frac{d\phi}{dy} \right], \\ y &= \frac{p}{\gamma}, \quad \gamma = \sqrt{1 + (\delta p)^2}, \quad \delta = \frac{v_T}{c} = \sqrt{\frac{2T}{mc^2}}. \end{aligned}$$

with  $Z$  and  $c$  denoting the ion effective charge and the speed of light, respectively. Further details on the model can be found in Ref. [45] and references therein. The models for the velocity,  $V$ , and the diffusivity,  $D$ , in the equation governing the dynamics of  $r$  are

$$V(r) = V_0 \mathbb{1}_{\{r > r_D\}}, \quad D(r, p) = \frac{D_0}{2} [1 + f(r)] e^{-(p/\Delta p)^2}, \quad f(r) = \tanh \left( \frac{r - r_D}{W} \right). \quad (38)$$

In the calculations presented we use the following typical model parameters

$$\begin{aligned} Z = 1, \quad \tau = 10^5, \quad \delta = 0.042, \quad E = 0.3, \quad \bar{\nu}_{ee} = 1, \quad \bar{\nu}_T = 1 \\ r_D = 0.7, \quad W = 10^{-2}, \quad \Delta p = 20, \quad V_0 = 0.003, \quad D_0 = 10^{-4} \end{aligned} \quad (39)$$

The integration domain is  $p \in (p_{\min}, p_{\max})$ ,  $\theta \in (0, \pi)$ , and  $r \in (0, 1)$ . In this context, the probability of the exit time represents the probability that an electron located at  $r$  with momentum  $p$  and pitch angle  $\theta$ , “runs away” and exits the integration domain by crossing the  $p = p_{\max}$  boundary (entering a high energy region) at a time less than or equal to  $T_{\max}$ . Based on this interpretation, in this section we will refer to the probability of the exit time as the “runaway probability”,  $P_{RE}$ . For the calculations we use  $(p_{\min}, p_{\max}) = (2, 50)$ , and  $T_{\max} = 120$ .

Figures. 6 and 7 show the calculation of the runaway probability using a uniform grid, with blue (yellow) denoting  $P_{RE} \sim 0$  ( $P_{RE} \sim 1$ ) values. Since this is a 3D problem, the results are displayed in  $(p, \theta)$  planes for different radial cuts, and in  $(p, r)$  planes for different  $\theta$  cuts, at successive times. The relatively small value of the parameter  $W$  in the function  $f(r)$  introduces a sharp transition in the radial dependence of  $V$  and  $R$  at  $r = r_D$ , which creates a boundary layer in the runaway probability. Resolving this boundary layer using a uniform grid in  $r$  requires a significant reduction of the global grid spacing. In particular as shown in Fig. 6 using  $\Delta r_s = 0.1$  gives rise to an artificial spreading of the transition boundary separating the  $P_{RE} \sim 1$  and  $P_{RE} \sim 0$  regions. As shown in Fig. 7, to recover the expected sharpness of the transition boundary using a uniform grid requires reducing the global grid spacing to  $\Delta r_d = 0.0025$ . However, using a global reduction of the grid spacing is numerically expensive and not needed in the whole computation domain. As an alternative we show in Fig.8 how the use of a non-uniform grid can accurately resolve the boundary layer, by using a large spacing,  $\Delta r_s = 0.1$ , for  $r \in [0, r_D]$  and a small spacing,  $\Delta r_d = 0.0025$ , for  $[r_D, 1]$ .

To further test the accuracy of the proposed method, Fig. 9 shows the radial dependence of the runaway probability,  $P_{RE}$ , at  $\theta = 15^\circ$  and  $p = 25$ . Since there are not known analytical solutions, we use as reference a high resolution direct Monte-Carlo simulation using 10,000 particles. As Fig. 9 shows, the proposed method perfectly recovers the reference solution when using a non-uniform grid. Using a (same cost) uniform grid or a sparse-grid reduces the accuracy of the computation.

In the previous discussion, the coefficients of the SDE in (37) were assumed time independent. However, in the more realistic and physically relevant cases, both, the electric field and the collision operator are time dependent making Eqs.(36) non-autonomous. To illustrate and test the proposed algorithm in this case, we change the constants  $\bar{\nu}_T$ ,  $\bar{\nu}_{ee}$ ,  $\delta$ , and  $E$  in (39) to the functions

$$\bar{\nu}_T(t) = \sqrt{\frac{\hat{T}}{\tilde{T}}}, \quad \bar{\nu}_{ee}(t) = \left(\frac{\tilde{T}}{\hat{T}}\right)^{3/2} \frac{\ln \hat{\Lambda}}{\ln \tilde{\Lambda}}, \quad \delta(t) = \sqrt{\frac{2\hat{T}}{mc^2}}, \quad E(t) = E_0 \left[\frac{\hat{T}_0}{\hat{T}}\right]^{3/2}, \quad (40)$$

where the time dependence enters through the function  $\hat{T}(t) = \hat{T}_f + (\hat{T}_0 - \hat{T}_f) e^{-t/t_*}$ ,  $mc^2$  is the rest mass of the electron,  $\ln \hat{\Lambda} = 14.9 - \frac{1}{2} \ln 0.28 + \ln \hat{T}$ , and  $\ln \tilde{\Lambda} = 14.9 - \frac{1}{2} \ln 0.28 + \ln \tilde{T}$ .

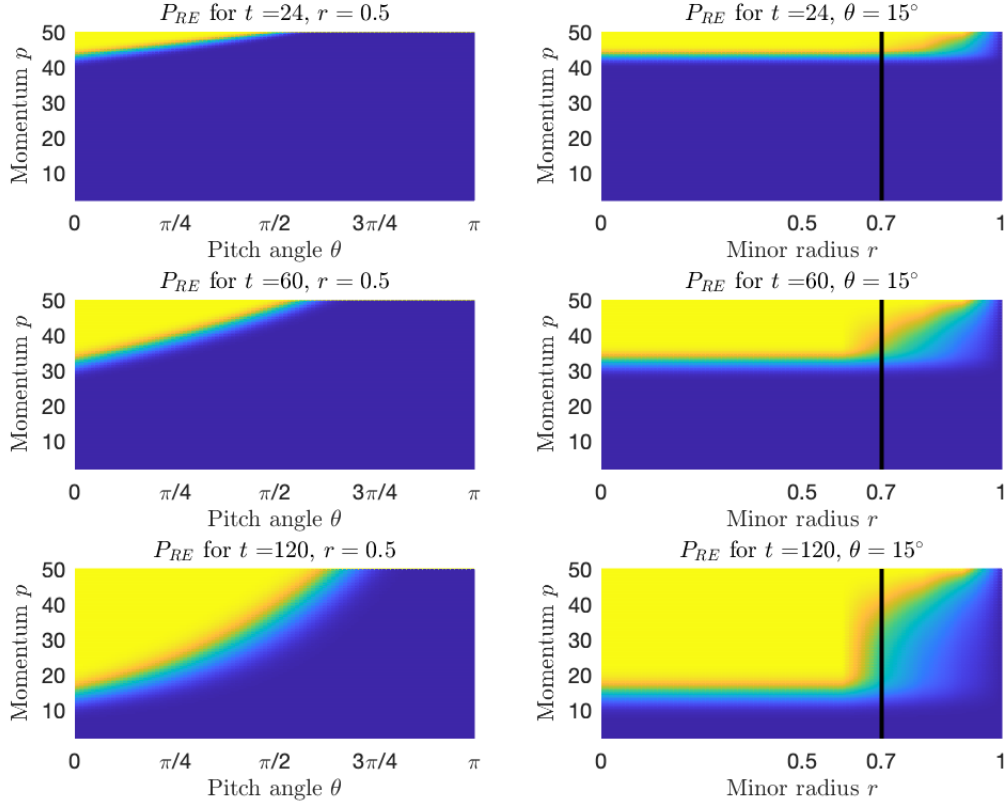


Figure 6: Computation of runaway probability,  $P_{RE}$ , using a *low resolution uniform grid* ( $\Delta r_s = 0.1$ ). Left column shows  $P_{RE}$  in the  $(\theta, p)$  plane at  $r = 0.5$ . Right column shows  $P_{RE}$  in the  $(r, p)$  plane at  $\theta = 15^\circ$ . The rows correspond to the three successive times  $t = 24, 60$ , and  $120$ . The use of a coarse grid leads to numerical diffusion causing an artificial spreading of the boundary separating the  $P_{RE} \sim 0$  (blue) and  $P_{RE} \sim 1$  (yellow) boundary around  $r = r_D = 0.7$  (black vertical line).

Physically, this model describes the generation of runaway electrons in dynamics scenarios of magnetic disruptions in which the plasma thermal quench, described with an exponential cooling model, generates a time dependent electric field described by Ohm's law using a Spitzer conductivity model. The constants  $\hat{T}_0$  and  $\hat{T}_f$  are the plasma temperature before and after the thermal quench,  $t_*$ , the cooling rate,  $E_0$  the pre-quench electric field, and  $\tilde{T}$  a reference temperature scale. As an example we consider the parameter values

$$\begin{aligned} Z = 1, \quad \tau = 6000, \quad E_0 = 10^{-3}, \quad \hat{T}_0 = 3, \quad \hat{T}_f = 0.005, \quad \tilde{T} = 3 \\ r_D = 0, \quad W = 10^{-4}, \quad \Delta p = 2, \quad V_0 = 0, \end{aligned} \quad (41)$$

and, to illustrate the dependence on time and radial diffusion, we vary the parameters  $t_*$  and  $D_0$ .

Figure 10 shows the time evolution of the density of seed runaway electrons,  $n_{RE}$ , at the

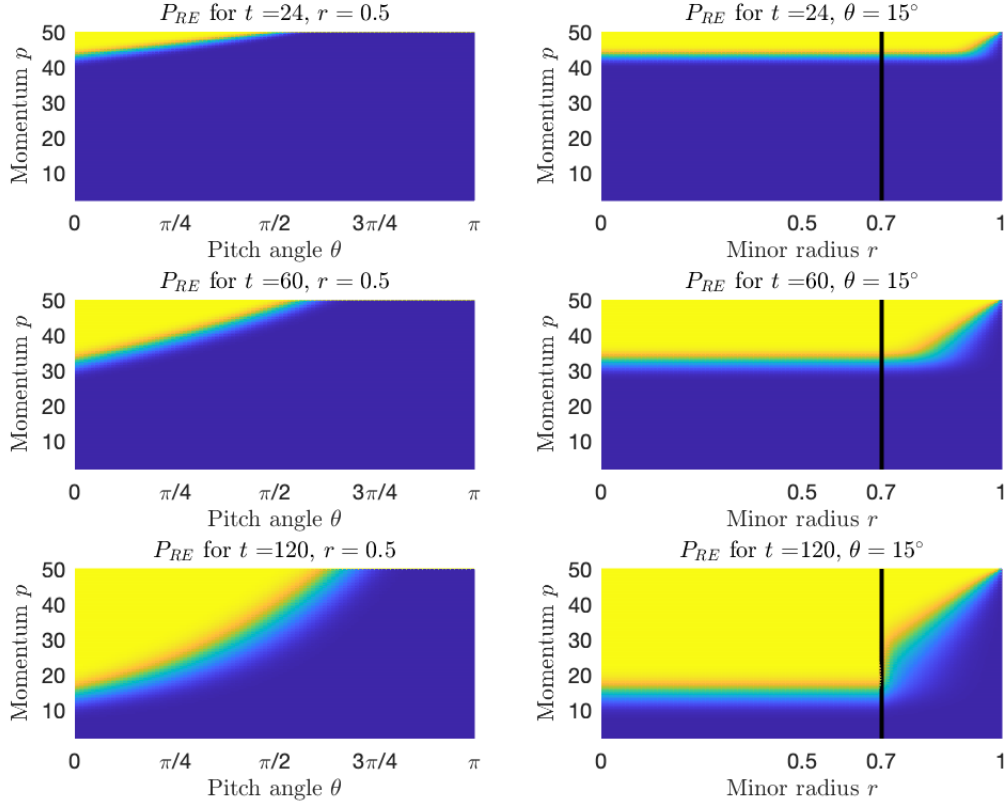


Figure 7: Same as Fig. 6 but using a *high resolution uniform grid* ( $\Delta r_d = 0.0025$ ). To eliminate the numerical diffusion shown Fig. 6 and recover the expected sharp transition between the  $P_{RE} \sim 0$  (blue) and  $P_{RE} \sim 1$  (yellow) boundary around  $r = r_D = 0.67$  (black vertical line) using a uniform grid requires a reduction of the grid spacing by more than two orders of magnitude. This global uniform refinement leads to a significant increase of the computational cost

fixed radius  $r = r_0 = 0.85$  defined as

$$n_{RE}(r_0, t) = 2\pi n_0 \int_{-1}^1 d\xi \int_0^\infty dp f_M(p) P_{RE}(\xi, p, r = r_0, t), \quad (42)$$

where  $n_0$  is the electron plasma density,  $f_M$ , is a Maxwellian distribution with temperature  $T_0$ , and  $P_{RE}(\xi, p, r = r_0, t)$  is the computed 3D, time dependent probability of runaway at  $r = r_0$ . Consistent with the runaway electron physics, it is observed that longer cooling rates (large  $t_*$ ) delay the onset of the seed runaway electrons production. In addition, as Fig. 11 shows,  $t_*$  and  $D_0$ , have a direct impact on the final saturation level of  $n_{RE}$ . As expected, fast cooling (small  $t_*$ ) leads to larger final saturation. On the other hand, increasing  $D_0$  results in smaller  $n_{RE}$  because radial diffusion deconfines a fraction of the electrons before they can be accelerated to runaway energies.

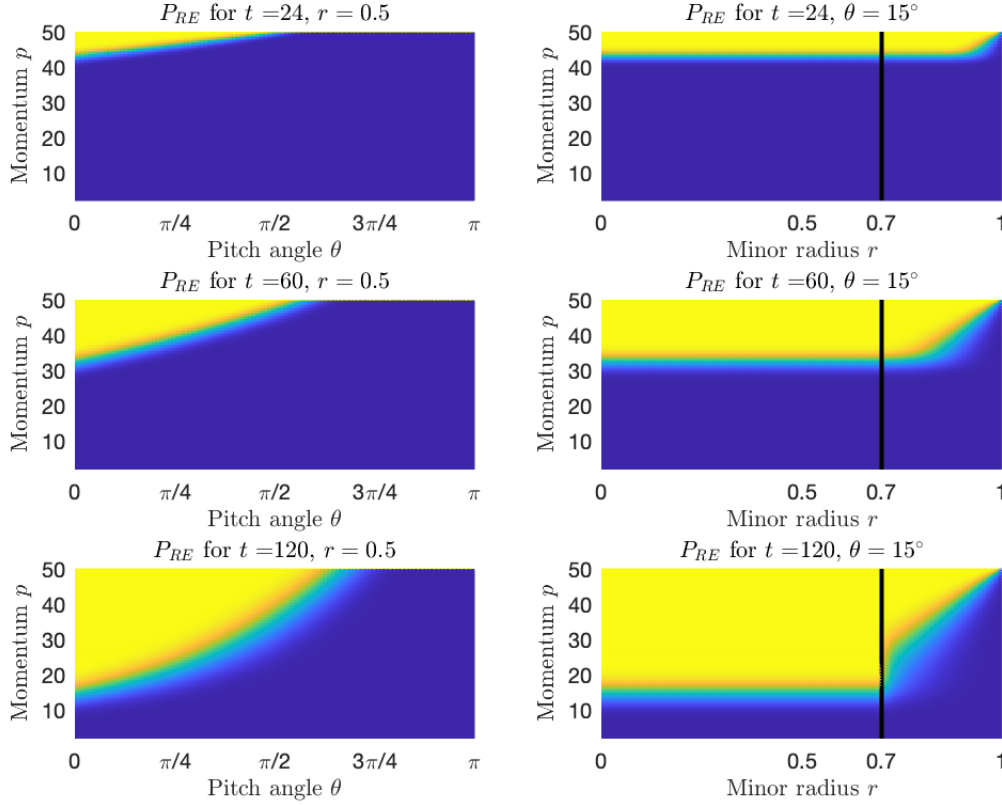


Figure 8: Same as Fig. 6, but using a *non-uniform grid*. The use of a grid with a large spacing,  $\Delta r_s = 0.1$ , for  $r \in [0, r_D]$ , and a small spacing,  $\Delta r_d = 0.0025$ , for  $[r_D, 1]$ , eliminates the numerical diffusion and recovers the expected sharp transition between the  $P_{RE} \sim 0$  (blue) and  $P_{RE} \sim 1$  (yellow) boundary around  $r = r_D = 0.67$  (black vertical line). The result is in agreement with that shown in Fig. 7 using a uniform fine grid, but the use of a non-uniform grid significantly reduces the computational cost.

## 5. Concluding Remarks

We have presented an accurate and efficient method for the computation of the exit time probability for a given system of non-autonomous (time-dependent) stochastic differential equations. The proposed numerical scheme can calculate this probability simultaneously for batches of particles with different initial condition and it is therefore straightforward to parallelize. The theoretical foundation of the proposed method is the Feynman-Kac formula that links the probability of exit time to the solution of the adjoint Fokker-Planck equation. We express the conditional expectations as integrals evaluated using Gauss-Hermite quadrature rules and pchip interpolation strategies, which can achieve first-order convergence rate. To compute the full time evolution of the exit time probability by using a single run of the algorithm we formulate the numerical scheme in matrix form.

We presented three examples illustrating specific aspects and advantages of the proposed numerical method. The first example considered the exit time probability in a standard 1D Brownian motion and illustrated the convergence properties of our approach as well as the efficiency of the GPU-accelerated algorithm. The second example considered the exit time



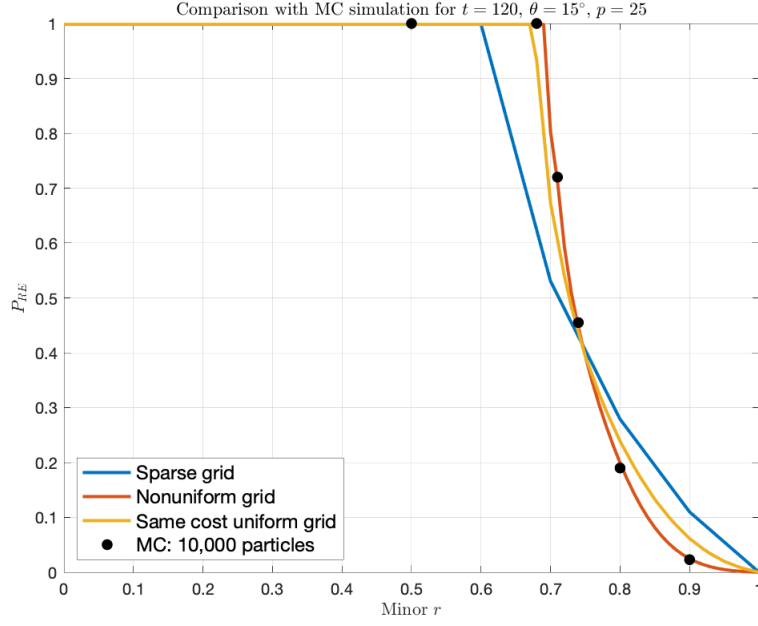


Figure 9: Radial dependence of the runaway probability,  $P_{RE}$ , at  $\theta = 15^\circ$  and  $p = 25$ . The black dots correspond to a high resolution direct Monte-Carlo simulation using 10,000 particles. The proposed method perfectly recovers in a numerically efficient way this direct expensive reference solution when using a non-uniform grid. Using a (same cost) uniform grid or a sparse-grid reduces the accuracy of the computation.

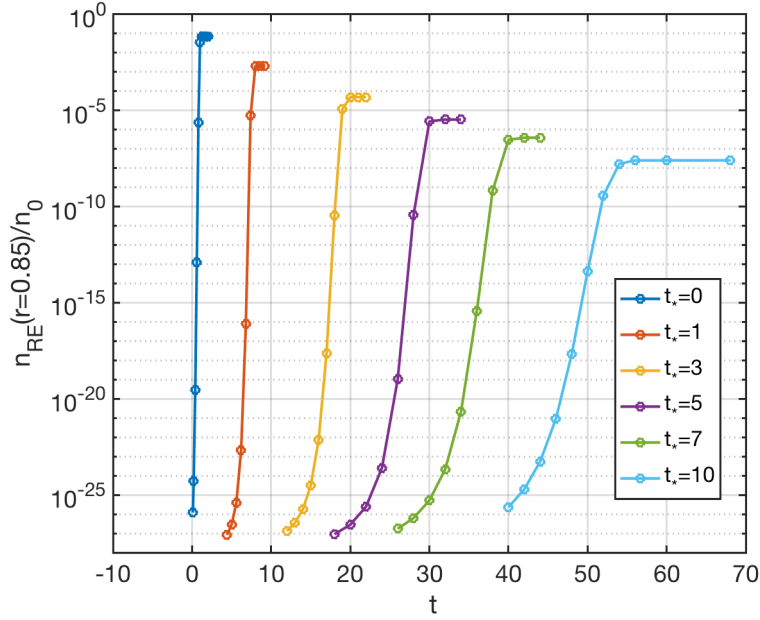


Figure 10: Dependence of time evolution of seed runaway electron density,  $n_{RE}$  at  $r_0 = 0.85$  (normalized to the plasma density,  $n_0$ ) on cooling rate time scale,  $t_*$ , for  $D_0 = 0.01$ .

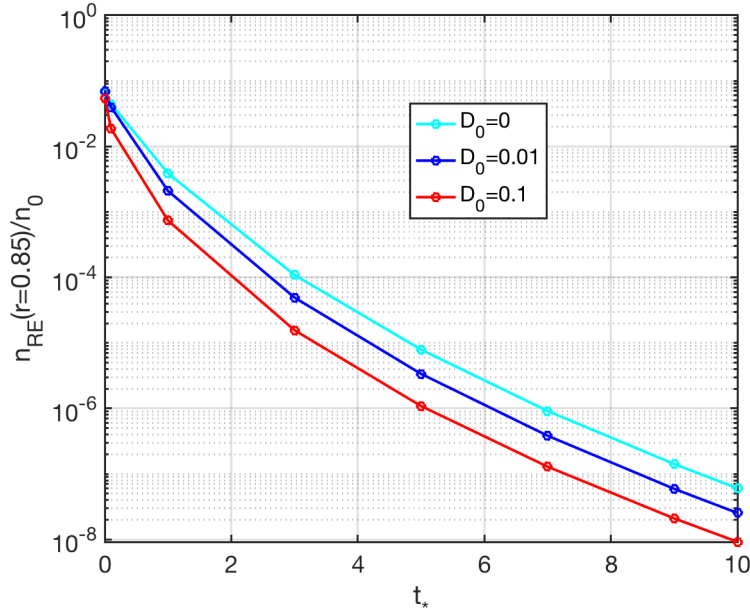


Figure 11: Dependence of final seed runaway electron density,  $n_{RE}$  at  $r_0 = 0.85$  (normalized to the plasma density,  $n_0$ ) on cooling rate time scale,  $t_*$ , and radial diffusivity,  $D_0$ .

in a 2D advection-diffusion problem with a time dependent incompressible fluid velocity field. This example showed that our numerical scheme is more optimal than the finite difference method regarding stability, accuracy, and computational cost. The third example presented a 3D plasma physics motivated problem and illustrated the seamless incorporation of nonuniform spatial grids in our scheme and the versatility of the method to solve complex physics problems demanding nontrivial temporal-spatial discretizations.

Our next step is to extend the proposed method to enable its use in more complex problems involving the coupling of SDEs models with already existing simulators describing parameters in the SDEs and/or external degrees of freedom. For example, in the plasma physics problem discussed in Sec. 4.3 the electric field,  $E$ , is taken as a fixed parameter. However, in reality, the spatio temporal evolution of  $E$  is governed Maxwell's equations, and it is thus important to extend the method to incorporate the coupling of the SDEs with a PDE solver for  $E$ . In this plasma physics problem there is also the need to go beyond the simplified radial diffusion model used in Sec. 4.3 and incorporate advanced models for the spatial evolution of the electrons. This task, which is quite challenging in the context of PDE based methods, can be accomplished by replacing the Euler scheme in (11) with the temporal propagators provided by the external particle simulator.

## Acknowledgements

This material is based upon work supported in part by the U.S. Department of Energy, Office of Science, Offices of Advanced Scientific Computing Research and Fusion Energy Science, and by the Laboratory Directed Research and Development program at the Oak Ridge National Laboratory, which is operated by UT-Battelle, LLC, for the U.S. Department

of Energy under Contract DE-AC05-00OR22725.

## References

- [1] H. Aref. The development of chaotic advection. *Physics of Fluids*, 14(4):1315–1325, 2002.
- [2] R. A. Bagnold. *An approach to the sediment transport problem from general physics*. US government printing office, 1966.
- [3] P. Baldi et al. Exact asymptotics for the probability of exit from a domain and applications to simulation. *The Annals of Probability*, 23(4):1644–1670, 1995.
- [4] F. Bernal and J. A. Acebrón. A comparison of higher-order weak numerical schemes for stopped stochastic differential equations. *arXiv preprint arXiv:1511.07195*, 2015.
- [5] R. B. Bird. Transport phenomena. *Appl. Mech. Rev.*, 55(1):R1–R4, 2002.
- [6] J. R. Brannan, J. Duan, and V. J. Ervin. Escape probability and mean residence time in random flows with unsteady drift. *Mathematical Problems in Engineering*, 7, 2001.
- [7] F. Buchmann. Computing exit times with the euler scheme. In *Research Report/Seminar für Angewandte Mathematik*, volume 2003. Seminar für Angewandte Mathematik, Eidgenössische Technische Hochschule, 2003.
- [8] F. M. Buchmann. Simulation of stopped diffusions. *Journal of Computational Physics*, 202(2):446–462, 2005.
- [9] L. Carbajal, D. del Castillo-Negrete, D. Spong, S. Seal, and L. Baylor. Space dependent, full orbit effects on runaway electron dynamics in tokamak plasmas. *Physics of Plasmas*, 24(4):042512, 2017.
- [10] S. Chandrasekhar. *Hydrodynamic and hydromagnetic stability*, oxford university press, oxford, 1961.
- [11] D. del Castillo-Negrete, L. Carbajal, D. Spong, and V. Izzo. Numerical simulation of runaway electrons: 3-d effects on synchrotron radiation and impurity-based runaway current dissipation. *Physics of Plasmas*, 25(5):056104, 2018.
- [12] J. Durbin. The first-passage density of a continuous gaussian process to a general boundary. *Journal of Applied Probability*, pages 99–122, 1985.
- [13] B. Ferebee. The tangent approximation to one-sided brownian exit densities. *Zeitschrift für Wahrscheinlichkeitstheorie und verwandte Gebiete*, 61(3):309–326, 1982.
- [14] B. Ferebee. An asymptotic expansion for one-sided brownian exit densities. *Zeitschrift für Wahrscheinlichkeitstheorie und Verwandte Gebiete*, 63(1):1–15, 1983.
- [15] M. I. Freidlin. *Functional integration and partial differential equations*. Number 109. Princeton university press, 1985.

- [16] M. I. Freidlin. *Functional Integration and Partial Differential Equations.(AM-109), Volume 109*. Princeton university press, 2016.
- [17] F. N. Fritsch and R. E. Carlson. Monotone piecewise cubic interpolation. *SIAM Journal on Numerical Analysis*, 17(2):238–246, 1980.
- [18] E. Gobet. Weak approximation of killed diffusion using euler schemes. *Stochastic processes and their applications*, 87(2):167–197, 2000.
- [19] E. Gobet and S. Menozzi. Exact approximation rate of killed hypoelliptic diffusions using the discrete euler scheme. *Stochastic Processes and their Applications*, 112(2):201–223, 2004.
- [20] P. Lánský and V. Lánská. First-passage-time problem for simulated stochastic diffusion processes. *Computers in biology and medicine*, 24(2):91–101, 1994.
- [21] C. B. Moler. *Numerical computing with MATLAB*. SIAM, 2004.
- [22] NVIDIA. Cuda toolkit 4.2 cusparse library. Technical Report *PG – 05329 – 041\_v01*, NVIDIA Corporation, 2701 San Tomas Expressway Santa Clara, CA, 2012.
- [23] É. Pardoux. Backward stochastic differential equations and viscosity solutions of systems of semilinear parabolic and elliptic pdes of second order. In *Stochastic Analysis and Related Topics VI*, pages 79–127. Springer, 1998.
- [24] E. Pardoux and S. Peng. Backward stochastic differential equations and quasilinear parabolic partial differential equations. In *Stochastic Partial Differential Equations and Their Applications*, pages 200–217. Springer Berlin Heidelberg, Berlin/Heidelberg, 1992.
- [25] B. T. Park and V. Petrosian. Fokker-planck equations of stochastic acceleration: A study of numerical methods. *The Astrophysical Journal Supplement Series*, 103:255, 1996.
- [26] C. Park and F. Schuurmann. Evaluations of barrier-crossing probabilities of wiener paths. *Journal of applied Probability*, pages 267–275, 1976.
- [27] P. Patie and C. Winter. First exit time probability for multidimensional diffusions: A pde-based approach. *Journal of computational and applied mathematics*, 222(1):42–53, 2008.
- [28] G. Peskir. On integral equations arising in the first-passage problem for brownian motion. *The Journal of Integral Equations and Applications*, pages 397–423, 2002.
- [29] E. Platen and N. Bruti-Liberati. *Numerical Solution of Stochastic Differential Equations with Jumps in Finance*, volume 64 of *Stochastic Modelling and Applied Probability*. Springer Berlin Heidelberg, Berlin, Heidelberg, 2010.
- [30] A. Quarteroni, R. Sacco, and F. Saleri. *Numerical Mathematics*, volume 332. Springer Science Business Media &, 2007.

- [31] H. Risken. *Fokker-planck equation*. Springer, 1996.
- [32] J. Rubin. Transport of reacting solutes in porous media: Relation between mathematical nature of problem formulation and chemical nature of reactions. *Water resources research*, 19(5):1231–1252, 1983.
- [33] P. Salminen. On the first hitting time and the last exit time for a brownian motion to/from a moving boundary. *Advances in applied probability*, 20(2):411–426, 1988.
- [34] Z. Schuss. *Brownian Dynamics at Boundaries and Interfaces*. In Physics, Chemistry, and Biology. Springer Science & Business Media, Aug. 2013.
- [35] T. Solomon and J. P. Gollub. Chaotic particle transport in time-dependent rayleigh-bénard convection. *Physical Review A*, 38(12):6280, 1988.
- [36] B. Spencer and L. Bergman. On the numerical solution of the fokker-planck equation for nonlinear stochastic systems. *Nonlinear Dynamics*, 4(4):357–372, 1993.
- [37] M. Stoyanov. User manual: Tasmanian sparse grids. Technical Report ORNL/TM-2015/596, Oak Ridge National Laboratory, One Bethel Valley Road, Oak Ridge, TN, 2015.
- [38] V. Strassen et al. Almost sure behavior of sums of independent random variables and martingales. In *Proceedings of the Fifth Berkeley Symposium on Mathematical Statistics and Probability, Volume 2: Contributions to Probability Theory, Part 1*. The Regents of the University of California, 1967.
- [39] K. Uchiyama. Brownian first exit from and sojourn over one sided moving boundary and application. *Zeitschrift für Wahrscheinlichkeitstheorie und Verwandte Gebiete*, 54(1):75–116, 1980.
- [40] Y. Wang, H. Qin, and J. Liu. Multi-scale full-orbit analysis on phase-space behavior of runaway electrons in tokamak fields with synchrotron radiation. *Physics of Plasmas*, 23(6):062505, 2016.
- [41] J. Yang, G. Zhang, and W. Zhao. A First-Order Numerical Scheme for Forward-Backward Stochastic Differential Equations in Bounded Domains. *Journal of Computational Mathematics*, 36(2):237–258, 2018.
- [42] Y. Yang, Y. Huang, and Y. Zhou. Numerical solutions for solving time fractional fokker-planck equations based on spectral collocation methods. *Journal of Computational and Applied Mathematics*, 339:389–404, 2018.
- [43] H. Yoshioka, K. Unami, and T. Kawachi. Partial differential equation model for spatially distributed statistics of contaminant particles in locally one-dimensional open channel networks. *Tenth International Conference on Hydrosience and Engineering*, pages 1–24, 2012.

- [44] W. Young, A. Pumir, and Y. Pomeau. Anomalous diffusion of tracer in convection rolls. *Physics of Fluids A: Fluid Dynamics*, 1(3):462–469, 1989.
- [45] G. Zhang and D. del Castillo-Negrete. A backward monte-carlo method for time-dependent runaway electron simulations. *Physics of Plasmas*, 24(9):092511, 2017.
- [46] G. Zhang, W. Zhao, C. Webster, and M. Gunzburger. Numerical methods for a class of nonlocal diffusion problems with the use of backward SDEs. *Computers & Mathematics with Applications*, 71:2479–2496, June 2016.
- [47] W. Zhao, Y. Fu, and T. Zhou. New kinds of high-order multistep schemes for coupled forward backward stochastic differential equations. *SIAM Journal on Scientific Computing*, 36(4):A1731–A1751, 2014.
- [48] W. Zhao, Y. Li, and G. Zhang. A Generalized  $\Theta$ -Scheme for Solving Backward Stochastic Differential Equations. *Discrete and Continuous Dynamical Systems. Series B. A Journal Bridging Mathematics and Sciences*, 17(5):1585–1603, 2012.
- [49] W. Zhao, J. Wang, and S. Peng. Error estimates of the  $\theta$ -scheme for backward stochastic differential equations. *Discrete and Continuous Dynamical Systems. Series B. A Journal Bridging Mathematics and Sciences*, 12(4):905–924, Nov. 2009.

## Significance and novelty

We present an accurate and efficient numerical method for solving the full dynamics of the probability distribution, denoted by  $P(t, x)$ , of the first exit time of stochastic differential equations with time-dependent parameters. The first exit time is arguably one of the most natural and important transport problems, and this work is motivated by critical physics and engineering applications, i.e., the modeling of runaway acceleration of electrons in realistic plasma physics systems. The main novelty of the proposed method are

- (a) The unconditional stability for any  $\Delta t$ , first-order convergence with respect to  $\Delta t$ , and second-order convergence with respect to  $\Delta x$ ;
- (b) The output of our method can be used to obtain the exit probability of the SDE with different initial conditions by doing simple convolution;
- (c) Recovering the entire dynamics of the exit probability  $P(t, x)$  by only one temporal iteration, and easy implementation on GPUs.

To our knowledge, our method is the first one that possesses all the three features among existing methods for computing  $P(t, x)$ . In comparison, the MC methods have feature (c); the PDE solvers for the forward Fokker-Planck equations have feature (a), (c); the implicit PDE solvers for the backward (adjoint) Fokker-Planck equations have feature (a), (b); the explicit solvers for the backward (adjoint) Fokker-Planck equations have feature (b), (c).